Three-dimensional velocity obstacle method for UAV uncoordinated avoidance maneuver

Jenie, Yazdi; van Kampen, EJ; de Visser, CC; Ellerbroek, J; Hoekstra, JM

DOI
10.2514/6.2016-1629

Publication date
2016

Document Version
Accepted author manuscript

Published in
Proceedings of the AIAA guidance, navigation, and control conference

Citation (APA)
Jenie, Y., van Kampen, EJ., de Visser, CC., Ellerbroek, J., & Hoekstra, JM. (2016). Three-dimensional velocity obstacle method for UAV uncoordinated avoidance maneuver. In *Proceedings of the AIAA guidance, navigation, and control conference: 4-8 January 2016, San Diego, California, USA* (pp. 1-16). Article AIAA 2016-1629 American Institute of Aeronautics and Astronautics Inc. (AIAA). https://doi.org/10.2514/6.2016-1629

Three-Dimensional Velocity Obstacle Method for UAV's Uncoordinated Avoidance Maneuver

Yazdi I. Jenie* Erik-Jan van Kampen† Coen C. de Visser‡ Joost Ellerbroek§ Jacco M. Hoekstra¶

Control and Simulation Section, Faculty of Aerospace Engineering, Delft University of Technology

This paper proposes a novel avoidance method called the Three-Dimensional Velocity Obstacle (3DVO) method. The method is designed for an Unmanned Aerial Vehicle (UAV) applications, in particular to autonomously handle non-cooperative encounters in an integrated airspace, by exploiting the limited space in three-dimensional manner. The method is a three-dimensional extension of the Velocity Obstacle method that can reactively generate an avoidance by changing the vehicle velocity vector based on the encounter geometry. Obstacle adverse maneuvers are anticipated by introducing the concept of the buffer velocity set that ensure ownship divergence from the obstacle before collision. While three-dimensional resolution is generated by choosing a right Avoidance Plane for the UAV to conduct a turning maneuver. Implementation of the 3DVO method is successfully tested in several simulations that demonstrate its capability to resolve various conflicts. A validation using Monte Carlo simulations is also conducted for a stressful 'super-conflict' scenarios, which result in zero collision for the entire samples.

Nomenclature

BZ	Buffer Velocity set
CC	Collision Cone set
DIV	Diverging Zone
$\mathbf{P}_\phi$	Avoidance Plane at the angle ϕ
$\mathbf{S_{pz}}$	Protected Zone
VO	Velocity Obstacle set
$\mathbf{VO}_\phi$	Velocity Obstacle representation on Avoidance Plane-ϕ
ϕ	Dihedral angle of the avoidance-plane from the XY-plane, [-]
ψ_{oi}	Azimuth angle of the obstacle-i from the ownship, [-]
θ_{oi}	Elevation angle of the obstacle-i from the ownship, [-]
θ_{vo}	Opening angle of the Velocity Obstacle Cone, [m]
$\vec{A}_{vo}$	Apex position of the Velocity Obstacle cone [m]
$\vec{C}_{vo}$	Base center position of the Velocity Obstacle cone [m]
$\vec{D}_{vo}$	Velocity Obstacle cone symmetric axis vector [m]
$\vec{V}_i$	Obstacle velocity vector [m/s]
$\vec{V}_o$	Ownship velocity vector [m/s]
$\vec{V}_R$	Relative velocity between the ownship and the obstacle, [m/s]
$\vec{V}_{avo}$	Avoiding velocity vector [m/s]
$\vec{X}_i$	Obstacle position relative to the ownship [m]
$\vec{X}_o$	Ownship position [m]
B_{vo}	Base of the Velocity Obstacle cone [m]

*PhD Student, Faculty of Aerospace Engineering, Delft University of Technology, 2629HS, Delft, The Netherlands
†Assistant Professor, Faculty of Aerospace Engineering, Delft University of Technology, 2629HS, Delft, The Netherlands
‡Assistant Professor, Faculty of Aerospace Engineering, Delft University of Technology, 2629HS, Delft, The Netherlands
§Assistant Professor, Faculty of Aerospace Engineering, Delft University of Technology, 2629HS, Delft, The Netherlands
¶Professor, Faculty of Aerospace Engineering, Delft University of Technology, 2629HS, Delft, The Netherlands

d_{avo}	Avoidance starting distance [m]
d_{oi}	Distance between the ownship and the obstacle-i [m]
d_{vo}	Length of the Velocity Obstacle cone [m]
r_{pz}	Radius of the Protected Zone [m]
r_{vo}	Base radius of the Velocity Obstacle cone [m]

I. Introduction

For Unmanned Aerial Vehicles (UAV) to be integrated into the airspace system, they are required to have an autonomous Conflict Detection and Resolution (CD&R) system that can demonstrate an adequate level of safety during its operation. In this context, as part of the air traffic, a UAV can encounter dynamic obstacles, such as manned aircraft and other UAVs. These encounters can be either cooperative,[?,1] or non-cooperative. In the latter situation, there is a chance that a UAV encounters a non-cooperative vehicle that might not avoid, move in an unpredicted way, or in the worst case, actually seek collision (hostile).

These kind of situations can only be detected independently by relying on on-board sensors of the vehicle, since the counterparts do not cooperatively share their flight data. As the result, the space for avoidance will be limited by the sensor range of detection, which is usually shorter than dependent surveillance, such as an Automatic Dependent Surveillance Broadcast system. The resolution maneuver, therefore, needs to fully exploit the remaining three-dimensional space, while anticipating the possible movement of the counterpart vehicles. The maneuver also needs to be aggressive to reach safety as fast as possible, possibly neglecting any original mission or trajectory. Ref.**?** describes this type of avoidance as an escape maneuver.

Reactive collision avoidance methods are potentially the most suitable methods to support an autonomous escape maneuver. These methods rely on the instantaneous situation to decide the avoidance maneuver, instead of relying on predetermined data or extensive prediction. this way, these methods are able to provide avoidance solutions in a dynamic environment, as fast as possible. Several reactive avoidance methods can be found in literature, including the Potential Field method,[?] and Geometric guidance methods such as the Collision Cone[?,?] or the Velocity Obstacle method.[?,?,?,2–7]

Most of those methods, however, generate resolution maneuvers only in two-dimensions, even when handling a three-dimensional encounters. The work of **?**, and **?** are among the few that demonstrate a method that handles encounters and generates resolutions in three-dimensions. Some of the methods are only demonstrated in a situation when the counterpart vehicles are not maneuvering. The work of 8 and 7 are two examples that consider a maneuvering obstacle, but in a reciprocal situation, where each vehicle uses the same avoidance algorithm. The work of **?** presents a Selective Velocity Obstacle method that handles heterogeneous multiple encounters that demonstrate a random maneuver of the obstacle, but the resolution is based on implicit coordination.

This paper proposes a novel avoidance method called the Three-Dimensional Velocity Obstacle method (3DVO), designed to handle uncoordinated encounters by exploiting the limited space for avoidance reactively, and in a three-dimensional manner. Counterpart adverse movements are considered as well to completely handle the encounter situation in the Escape Layer described in **?**. The 3DVO method is an extension of the Velocity Obstacle method (VO-method) that can reactively generate an avoidance maneuver by changing the vehicle velocity vector, based on the encounter geometry, as can be observed in Figure 1. The work of Fiorinni[2] is among the first that introduces the concept, while the application of the method for UAVs can be found in Ref.**?** and **?**.

This paper is structured as follows. Section II discusses the concept of the 3DVO by introducing the translation of the original VO-method into three-dimensions. The approaches to handle the maneuvering obstacle are elaborated as well, along with the introduction of the Avoidance Planes concept. After that, Section III explains the possible strategies for the 3DVO, which include the avoidance algorithm, the decision process in choosing the Avoidance Plane, and the derivation of the avoidance turning rate. Section IV presents the implementation of the three-dimensional VO-method in several simulations, where the method performance is demonstrated. A validation process using Monte Carlo simulation is also conducted and presented in this section. Section V ends the paper with several concluding remarks.

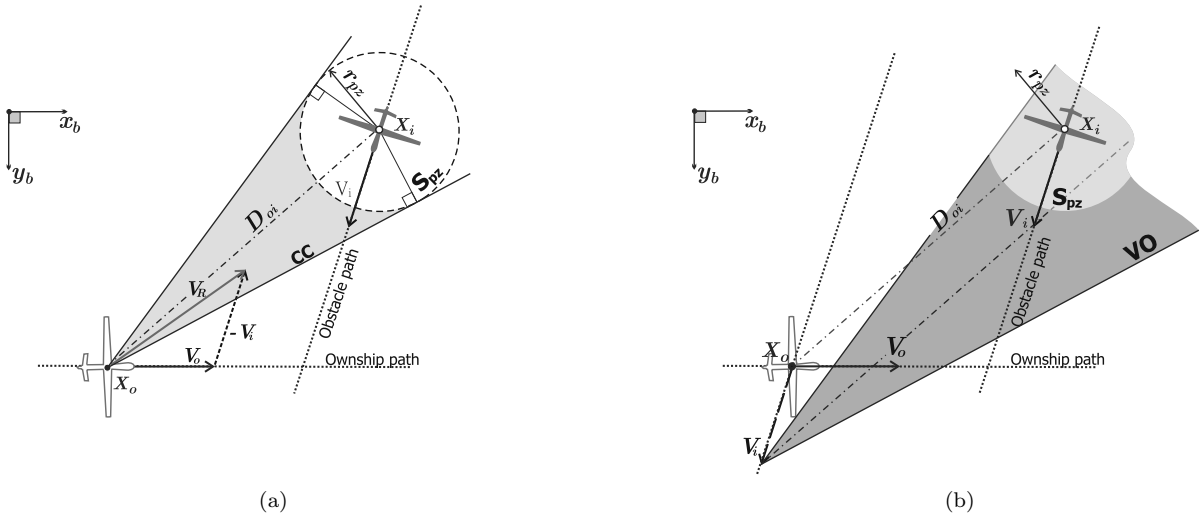

Figure 1. Graphical presentation of (a) Collision Cone and (b) The Velocity Obstacle method

II. Three-dimensional Velocity Obstacle Method

The Three-dimensional Velocity Obstacle method (3DVO) extends the use of the original VO-method,[?,2] which is applied in a two dimensional encounter, such as shown in Figure 1-a. In every encounter case, a collision cone set (**CC**) can be drawn, which collects all relative velocity vector between the vehicles, that intersect the protected zone (S_{pz}), a threshold area around the obstacle. Whether the two vehicle are bound to collide or not, therefore, can be determined by the inclusion of their relative velocity $\vec{V}_R$ to the **CC**. The VO-method uses the inclusion of the ownship absolute velocity vector $\vec{V}_o$ into the so-called Velocity Obstacle set (**VO**), which is the translation of **CC** along the velocity of the obstacle, $\vec{V}_i$, as shown in Figure 1-b. To avoid the obstacle, the ownship need to change its velocity vector to a point outside the **VO**. A diverging zone **DIV**, half-area separated by the $\vec{V}_i$ vector, is also added to determined whether the two vehicle are immediately diverging from each other.

The VO-method extension into the 3DVO includes the detection of three-dimensional conflicts, and the generation of possible avoiding route that also exploit the three-dimensional space around the ownship. This section explains the detection part by converting the sets of the VO-method to a three-dimensional definition. The generation of avoiding routes, along with the strategy for avoidance, is explained in the section afterward.

A. 3DVO Velocity Obstacle Cone

The concept of the VO-method is extended for three-dimensional cases by first redefining the protected zone, S_{pz}, from a circle to a three-dimensional form. There are two types of S_{pz} that can be found in the literature, either spherical,[?] or cylindrical.[?,?] This paper uses the spherical protected zone definition, since it can represent UAV encounters and resolutions better in the three-dimensional space. The reason is that unlike manned-flight, a UAV is much more agile: it can have a trajectory an dconduct avoidance in any direction in any direction exploiting the entire space around it. A spherical protected zone will treat obstacles equally regardless of the direction.

Consider a three dimensional encounter case between an avoiding vehicle, or an own-ship, and an obstacle, as depicted in figure 2. Similar to the two-dimensional case, the Collision Cone **CC** can be derived by collecting every relative velocity $\vec{V}_R$ whose positive elongation intersects the S_{pz} sphere. In this three-dimensional case, the **CC** takes the shape of a right-cone with size and orientation corresponding to the dimension of $\mathbf{S_{pz}}$ and the obstacle position $\vec{X}_i$, relative to the own-ship. The apex of **CC** is the ownship position $\vec{X}_o$, where every tangential line from $\vec{X}_o$ to the $\mathbf{S_{pz}}$ is a generating line of the cone (generatrix).

Similar to the two-dimensional case, the Velocity Obstacle set is obtained by translating the **CC** cone in three-dimensions along the $\vec{V}_i$ from X_o, as shown in Figure 2-b. With this set, the collision criterion between

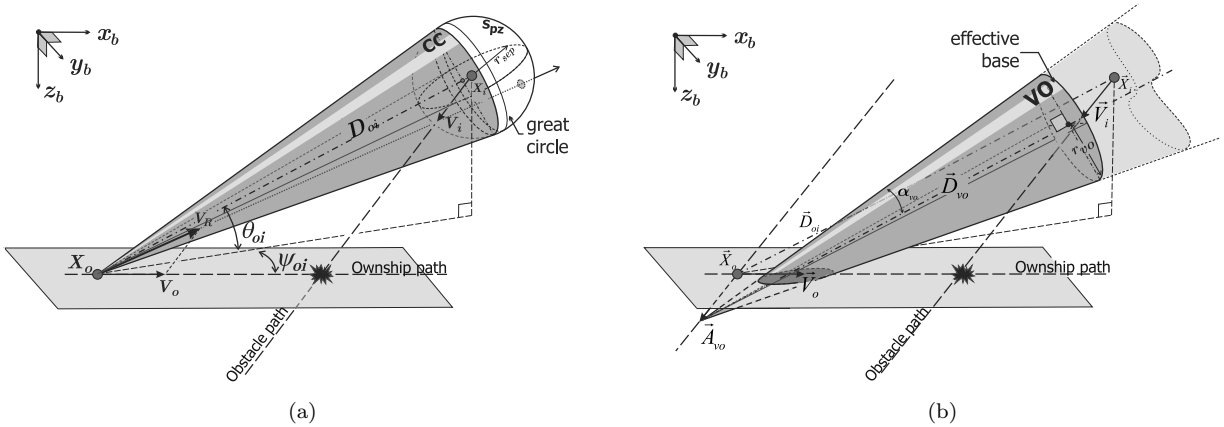

Figure 2. Three dimensional velocity obstacle set definition. (a) the Collision Cone CC, (b) Translated CC cone to the Velocity Obstacle set VO

two vehicles in three-dimensional space can be defined: an ownship will eventually collide if, and only if, its velocity vector $\vec{V}_o$ is included in the corresponding **VO** cone, such as $\vec{V}_o \in \mathbf{VO}$.

As a right cone, the three-dimensional **VO** can be defined by three parameters, i.e., the position of its apex, $\vec{A}_{vo}$, the position of the center of its base $\vec{C}_{vo}$, and the radius of the base, r_{vo}. These parameters are mathematically expressed in equations (2)-(3), by first defining the obstacle position in spherical coordinates (distance d_{oi}, elevation θ_{oi}, and azimuth ψ_{oi}) with respect to the ownship frame of reference in equation (1). Notice that the base of the VO cone, denoted as B_{vo}, does not coincide with the great circle of S_{pz}. The $\vec{D}_{vo}$ is used as a notation for the vector of the **VO** symmetric axis, connecting $\vec{A}_{vo}$ and $\vec{C}_{vo}$.

$$d_{oi} = \left|\vec{X}_i\right| = \sqrt{x_i^2 + y_i^2 + z_i^2}, \qquad \theta_{oi} = \arccos\left(\frac{z_i}{d_{oi}}\right), \qquad \psi_{oi} = \arctan\left(\frac{z_i}{x_i}\right) \tag{1}$$

$$d_{vo} = \frac{d_{oi}^2 - r_{pz}^2}{d_{oi}}, \qquad r_{vo} = r_{pz}\frac{\sqrt{d_{oi}^2 - r_{pz}^2}}{d_{oi}}, \qquad \theta_{vo} = \arctan\left(\frac{r_{vo}}{d_{vo}}\right) \tag{2}$$

$$\vec{A}_{vo} = X_o + V_i, \qquad \vec{D}_{vo} = \begin{bmatrix} \cos\theta_{oi}\cos\psi_{oi} \\ \cos\theta_{oi}\sin\psi_{oi} \\ \sin\theta_{oi} \end{bmatrix} d_{vo}, \qquad \vec{C}_{vo} = \vec{A}_{vo} + \vec{D}_{vo} \tag{3}$$

Similar to the two-dimensional case, the inclusion of the $\vec{V}_o$ vector end point in the **VO** cone can be determined by checking the angle between the vector from the cone apex $\vec{A}_{vo}$, and the cone symmetrical axis. Equation (4) represents the criteria of inclusion using the vector dot product. The second criterion in equation (4) is required to make sure the $\vec{V}_o$ point is in the correct half (nappe) of a cone in euclidean space. The third term is to ensure the imminence of the encounter by the avoidance starting point, d_{avo}, since the first two criteria are unbounded: they represent the collision occurrence within infinite time in the future.

$$\vec{V}_o \in \mathbf{VO}_i \iff \left\{ \arccos\left(\frac{\left[\vec{V}_o - \vec{A}_{vo}\right] \cdot \vec{D}_{vo}}{\left|\vec{V}_o - \vec{A}_{vo}\right| d_{vo}}\right) < \theta_{vo} \quad \wedge \quad [\vec{V}_o - \vec{A}_{vo}] \cdot \vec{D}_{vo} > 0 \quad \wedge \quad d_{oi} < d_{avo} \right\} \tag{4}$$

The **VO** cone expands as the two vehicles converge, and shrinks as they diverge. When the θ_{vo} reaches $\pi/2$, the ownship position is exactly on the surface of the protected zone $\mathbf{S_{pz}}$, or $d_{oi} = r_{pz}$, as indicated in equation (2). A degenerate case happens when $d_{oi} < r_{pz}$, in which case the **VO** cone cannot be defined. This indicates the collision between the vehicles that must be prevented.

Finally, multiple encounters are accommodated in the three-dimensional setup by taking the summation of the **VO** sets and the intersection of the **DIV** sets. Let $i = 1, 2, 3, ..., N$ be the number assignment of N-imminent obstacles under consideration, and the overall $\mathbf{VO}^+$ for a multiple encounter case is the union

of the Velocity Obstacle set, or $\bigcup_i \mathbf{VO}_i$. The ownship velocity vector is included in the overall set if it is included in at least one of the VO_i, or,

$$\vec{V}_o \in \bigcup_i \mathbf{VO}_i \iff \exists i : \vec{V}_o \in \mathbf{VO}_i \tag{5}$$

B. Handling Maneuvering Obstacles: The Buffer Velocity Set

The problems in using the VO-method in situations where the obstacles are maneuvering has been addressed in previous studies. The work of 7 describes the problem of oscillation and the reciprocal dance in cases of two dimensional conflicts, where each of the vehicle attempts avoidance using the VO-method. These problems, which eventually cause a failed avoidance, are solved using an implicit coordination of avoidance.[?,7] However, if those methods are tested in an uncoordinated situation, the problems reappear with an addition of another problem: a sudden inclusion. This latest problem, also included in the 'domino effects',[9] occurs when a vehicle adversely changes its course in a close proximity with another vehicle.

An extra set can be added to the Velocity Obstacle set, in order to handle the possible maneuver of the obstacle. Consider the case shown in Figure 3-a. Based on the encounter geometry, a VO set can be generated for the ownship to avoid the obstacle. However, within a time-step the obstacle can change its velocity vector, for example, by rotation within the range of V_i' to V_i''. For each of these 'arc's of velocity vectors, a new **VO** set can be defined, which, as shown in the figure, might ruled out the initial assumed safe zones.

If the possible maneuvers of the obstacle within a time step can be predicted or assumed, they can be anticipated by summing all the possible **VO** sets into one big set. Figure 3-a, for example, show this summation as the triangle that originated at point A^+, collecting all possible **VO**. The resulting triangular set, however, is not aligned with the axis of the original **VO**, and add an extra degree of freedom for the combined **VO** definition, especially in three dimensional cases.

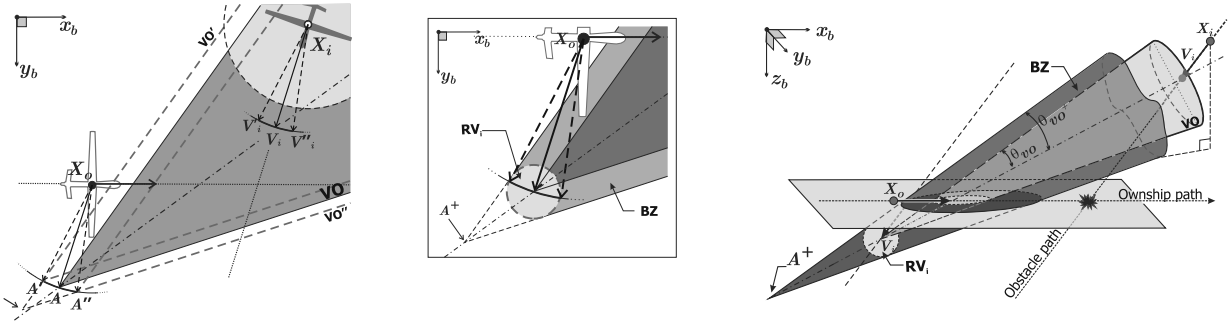

(a) (b) (c)

Figure 3. The Buffer Zone definition. (a) in two-dimensions, (b) in three-dimensions

Figure 3-b define a simpler definition for the sums of VOs, by using a circular reachable velocity set of the obstacle, RV_i. This set collects every possible 'arc' of V_i within a time step, from any arbitrary bearing angle between vehicles separated in a particular distance. The resulting sums of VO is then can be defined simply by moving the apex in the opposite direction of VO base until the entire RV_i is included. This also holds in the three dimensional setup, where the RV_i is represented as a sphere, as shown in the Figure 3-c. This paper denotes the extra layer of the **VO** as the Buffer Velocity set (**BV**). Furthermore, the combined **VO** resulted is denoted as the $\mathbf{VO}^+$, which effectively takes into account the obstacle maneuver within a time step.

The VO parameters in three dimension are therefore redefined, as expressed in equation (6) until (8). The radius of the $\mathbf{RV_i}$, the r_{rvi}, is expressed in equation (8), and it depends on the assumed value of the change of heading of expected obstacles within a time step, $\omega_i.\Delta t$.

$$d_{vo^+} = \frac{(d_{oi}+d_x)^2 - r_{pz}^2}{d_{oi}+d_x}, \qquad r_{vo^+} = r_{pz}\frac{\sqrt{(d_{oi}+d_x)^2 - r_{pz}^2}}{d_{oi}+d_x}, \qquad \theta_{vo^+} = \theta_{vo} \tag{6}$$

$$\vec{A}_{vo^+} = A_{vo} - \frac{D_{vo}}{d_{vo}} d_x, \qquad \vec{D}_{vo^+} = \frac{D_{vo}}{d_{vo}} d^+_{vo}, \qquad \vec{C}_{vo} = \vec{A}_{vo} + \vec{D}_{vo} \tag{7}$$

where,

$$r_{rvi} = V_i.\Delta t\sqrt{2\left(1-\cos(\omega_i.\Delta t)\right)}, \qquad d_x = d_{oi}\frac{r_{rvi}}{r_{pz} - r_{rvi}} \tag{8}$$

Equation (9) presents the $\vec{V}_o$ inclusion criteria to the $\mathbf{VO}^+$. The inclusion into the BZ zone in particular, can be derived by the subtraction of **VO** (equation (4)) from $\mathbf{VO}^+$.

$$\vec{V}_o \in \mathbf{VO}^+ \iff \left\{ \arccos\left(\frac{\left[\vec{V}_o - \vec{A}_{vo^+}\right] \cdot \vec{D}^+_{vo}}{\left|\vec{V}_o - \vec{A}_{vo^+}\right| d^+_{vo}} \right) < \theta_{vo^+} \quad \wedge \quad [\vec{V}_o - \vec{A}_{vo^+}] \cdot \vec{D}_{vo} > 0 \quad \wedge \quad d_{oi} < d_{avo} \right\} \tag{9}$$

C. Avoidance Planes

Similar to the original VO-method, in order to avoid the obstacles, the ownship needs to update its velocity vector to a point outside every relevant VO sets, the Avoidance Velocities, $\vec{V}_{avo}$. In three-dimensional setup, these point of avoidance velocity become more complex to be determined with the more option of escaping routes horizontally, vertically, or in combination between the two. If the option of velocity updates of the ownship can be represented with a particular three-dimensional curve or a sphere, then the option of avoidance is the intersection of that curve with the VO cone. The analytical derivation of such intersection involves a complicated quartic equation, which defeat the purpose of the VO-method as a reactive and graphically understandable method for avoidance.

Therefore, the 3DVO is accompanied by the concept of Avoidance Planes, similar to the one introduced in the preceding paper.[?] This concept is used as a tool to logically and graphically describe the three-dimensional case into separate two-dimensional setups, and find the appropriate velocity for avoidance. Therefore, instead of trying to derived all the possible resolution for avoidance, the 3DVO focuses only on a finite number of avoidance planes, which can be predefined based on the vehicle performance. Ref **?** presents a similar method of three-dimensional case breakdown that are concentrated for two avoidance planes, the lateral plane (XY-Plane) and the longitudinal plane (XZ-Plane). The method presented in 10 also resembles the method with a very fine discretization of planes around the ownship X-axis.

The Avoidance Planes, P_ϕ, are defined as any plane in which lies the ownship velocity vector $\vec{V}_o$, as shown in figure 4-a. The avoidance is assumed to be conducted in one of these planes, which is parameterized by the angle of rotation of the plane, $\phi_{\mathbf{P}}$, around the vehicle X-axis. The **VO**, therefore, is represented as a two-dimensional cross sectional area, $\mathbf{VO}_{\mathbf{P}_\phi}$. Since the **VO** is a right-cone, the $\mathbf{VO}_{\mathbf{P}_\phi}$s are conic section, as shown in the example of four Avoidance Plane, where $\phi_{\mathbf{P}} = -90^o, -45^o, 0^o$ and 45^o, in figure 4-b. By comparing between the resulting $\mathbf{VO}_{\mathbf{P}_\phi}$, the own-ship can choose the best plane for an optimal avoidance.

The type of conic section can be determined by comparing the **VO**'s opening angle, θ_{vo} , with the acute dihedral angle between the avoidance plane $\mathbf{P}_\phi$ and the cone base-circle $\mathbf{B_{vo}}$. This angle, denoted as $\delta_{\mathbf{P}_\phi}$, can be derived as in the following equation (10). The types of conic section, therefore, can be summarized by the following list.

1. if $\delta_{\mathbf{P}_\phi} = 0$, then VO_P is **a circle**, if also $A_{vo} \in P_\phi$, then VO_P is a **single point**.
2. if $\delta_{\mathbf{P}_\phi} < \pi/2 - \theta_{vo}$, then VO_P is **an ellipse**, if also $A_{vo} \in P_\phi$, then VO_P is **a single point**.
3. if $\delta_{\mathbf{P}_\phi} = \pi/2 - \theta_{vo}$, then VO_P is **a parabolic area**, if also $A_{vo} \in P_\phi$, then VO_P is **a straight line**.
4. if $\delta_{\mathbf{P}_\phi} > \pi/2 - \theta_{vo}$ and P_ϕ does not cut through the VO-cone axes, then VO_P is **a hyperbolic area**, if also $A_{vo} \in P_\phi$, then VO_P is **a triangle**.

$$\delta_{P_\phi} = \arccos\left(\frac{\vec{D}_{vo}}{d_{vo}} \cdot \begin{bmatrix} 0 \\ \sin\phi_{\mathbf{P}} \\ \cos\phi_{\mathbf{P}} \end{bmatrix} \right) \tag{10}$$

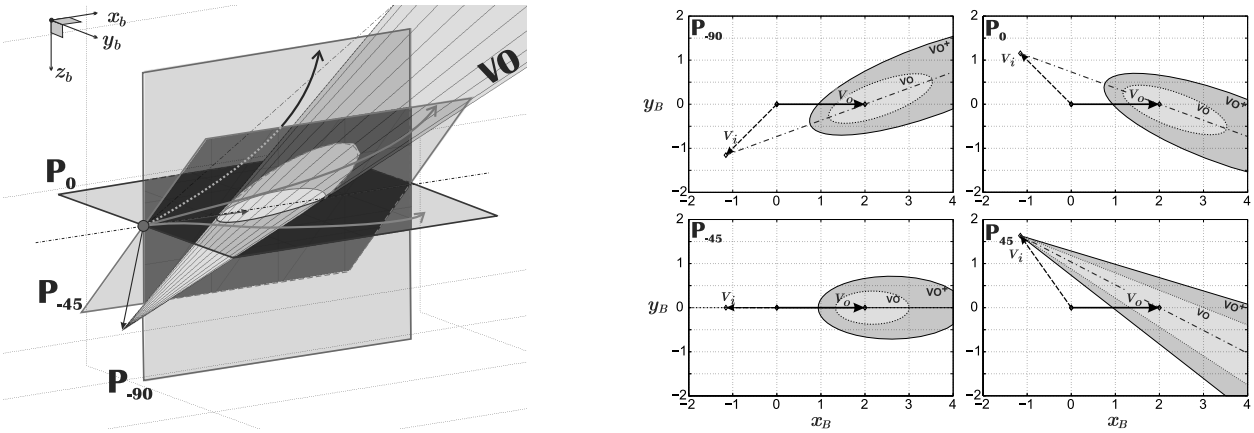

(a) (b)

Figure 4. The . (a) The avoidance plane. The ownship can choose its avoidance maneuver by moving in one selected plane, e.g. $\mathbf{P_0}$, $\mathbf{P_{60}}$, or $\mathbf{P_{90}}$. (b) Conic-sections of the $\mathbf{VO}^+$ cone and the DIV zone on several avoidance-planes. The thick arrow on the X-Axis represent $\vec{V}_o$.

As mentioned in the list, several degenerate cases can appear, where the resulting conic section is a point, a line, or two lines. Figure 4-b also show one example of the last degenerate case in the $\mathbf{P_{45}}$, where the conic section area is then defined by the triangle limited by the two intersecting lines of the $\mathbf{P_{45}}$ and the **VO** cone surface. In this case, if the center of the cone base, $\mathbf{C_{vo}}$, also lies on the avoidance plane along with the $\vec{V}_i$, the resulting conic section reverts the **VO** back to the two dimensional Velocity Obstacle.

To derive the conic-section in an arbitrary avoidance plane, this paper expresses the **VO** cone parameters using parametric equations in Euclidean space with respect to each plane frame of reference, as presented in equation (11) - (14). This way, the resulting velocity obstacle conic-sections, denoted as $\mathbf{VO}_{\mathbf{P}_\phi}$, is simplified as a polygon formed by a finite set of points on the limiting curves, determined by solving the x_{vo} and y_{vo} in equation (11) for $z_{vo} = 0$. This method for deriving the $\mathbf{VO}_{\mathbf{P}_\phi}$ is chosen instead of other method such as deriving the exact quadric functions due to its simplicity that suppress the required computational power. Moreover, it is also possible to use the parametric derivation of the $\mathbf{VO}_{\mathbf{P}_\phi}$ from a S_{pz} that shaped other than a sphere, as long as the points that form the base of the **VO** cone (or pyramid) is determined.

$$VO^+_{p_\phi} = \begin{bmatrix} x_{vo^+} \\ y_{vo^+} \\ z_{vo^+} \end{bmatrix} = R_{p_\phi} \left(R_{\theta_{oi}|\psi_{oi}} \begin{bmatrix} u \\ u\cos t \tan\theta_{vo^+} \\ u\sin t \tan\theta_{vo^+} \end{bmatrix} + \begin{bmatrix} V_{ix} \\ V_{iy} \\ V_{iz} \end{bmatrix} \right) \tag{11}$$

where,

$$0 \le t < 2\pi, \qquad u \ge 0 \tag{12}$$

$$R_{\theta_{oi}|\psi_{oi}} = \begin{bmatrix} \cos\psi_{oi}\cos\theta_{oi} & \sin\psi_{oi} & -\cos\psi_{oi}\sin\theta_{oi} \\ -\sin\psi_{oi}\cos\theta_{oi} & \cos\psi_{oi} & \sin\psi_{oi}\sin\theta_{oi} \\ \sin\theta_{oi} & 0 & \cos\theta_{oi} \end{bmatrix} \tag{13}$$

$$R_{P_\phi} = \begin{bmatrix} 1 & 0 & 0 \\ 0 & \cos\phi & \sin\phi \\ 0 & -\sin\phi & \cos\phi \end{bmatrix} \tag{14}$$

The parameter t in equation (11) is the free-parameter of the $\mathbf{VO}^+$ circular base, while u is the free-parameter of the generating lines of the cone, which is bounded to be equal or greater than zero to remove the other nappe of the cone. For hyperbolic section, this bound in some cases can omit a significant part of the section, and therefore an additional extrapolation function might be required to complete the $VO^+_{p_\phi}$

section until it covers the range reachable by the $\vec{V}_o$. The solution for $z_{vo} = 0$ will determine the value of u, as presented in the following equation (15).

$$u(t) = \frac{V_{iz}\cos\phi - V_{iy}\sin\phi}{(\sin\phi\cos\theta_{oi} + \cos\phi)\sin\psi_{oi} + ((\cos\phi\cos\theta_{oi} - \sin\phi\sin\psi_{oi}\sin\theta_{oi})\sin t - \sin\phi\cos\psi_{oi}\cos t)\tan\theta_{vo^+}} \tag{15}$$

The $\mathbf{VO}_\phi$ for the degenerate cases can also be indicated using the numerator and denominator of equation (15). If $V_{iz}\cos\phi - V_{iy}\sin\phi = 0$, or in other word, if $\tan\phi = \frac{V_{iz}}{V_{iy}}$, all **VO** generating lines cross the avoidance plane on its apex. In this case, the $\{x_{vo}, y_{vo}\}$ pair is determined by the t roots of the denominator. Two, one, or zero solutions can be obtained, which, together with the cone apex, will result in a $\mathbf{VO}_\phi$ set that takes a form of a triangle, a line, or a single point, respectively.

III. Strategy for a Three-dimensional Avoidance

The three-dimensional definition of the Velocity Obstacle sets and criteria in the previous section constructs the proposed 3-dimensional Velocity Obstacle method (3DVO). This section elaborate an example of a strategy in using those definitions to generate a reactive avoidance maneuver in three dimension. This strategy is resembles the two-dimensional avoidance strategy in Ref.,[?] with an additional step to select the safe Avoidance Plane.

A. Avoidance Algorithm

The algorithm of avoidance is defined according to the condition of the ownship velocity vector $\vec{V}_o$ with respect to the defined sets in 3DVO. Additionally, the velocity vector that directs the ownship back to its original goal, $\vec{V}_{goal}$ is also checked to determine the original mission safety after avoidance. The algorithm is presented graphically in Figure 5, differentiated as the three modes of mission, avoid, and maintain.

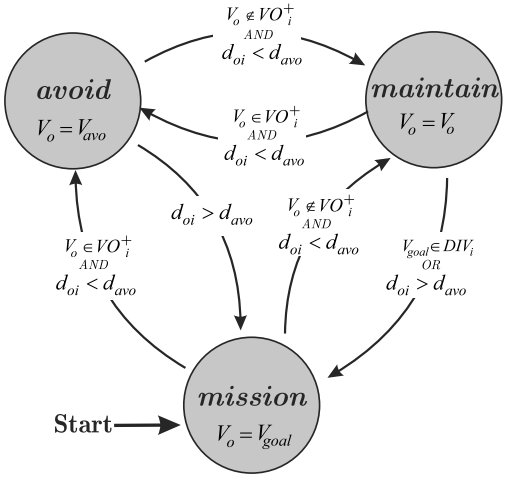

Figure 5. the Three-dimensional Velocity Obstacle method algorithm.

From a condition where the velocity vector is heading towards a designated goal, $\vec{V}_o = \vec{V}_{goal}$, whenever the $\vec{V}_o$ is included in the corresponding **VO**, or fulfilling equation (4), the ownship goes to the avoid mode. If it is imminent but not included in either the **VO** set, the ownship can keep its heading towards its original goal in the maintain-mode. In the avoiding mode the $\vec{V}_o$ is updated continuously in the direction of the surface of the $\mathbf{VO}^+$ until it steps outside the set, where the ownship is then switches to maintain-mode. From the maintain mode, the ownship might need to switch back to the avoid-mode due to an obstacle maneuver, if the encounter is still imminent. Mission mode is restored whenever the encounters are no longer imminent, $d_{oi} > d_{avo}$.

In the avoid-mode, the ownship velocity vector is updated in order to get outside of the velocity obstacle set $\mathbf{VO}^+$. In the VO-method, the direction of the velocity updates commonly follows a point on the **VO**

surface, denoted as the possible avoidance velocity, $\vec{V}_{avo}$. This point can be chosen based on various strategies, such as by accelerating or decelerating while staying on the path, by turning without alteration of speed, or by simply choosing a closest point from the current velocity. This paper focuses on the second strategy, to provide an escape route by turning in with a certain rate, ω_{avo}, without altering the speed.

By using the avoidance plane, the $\vec{V}_{avo}$ point is determined in each plane as the intersection point between the $\mathbf{VO}_{\mathbf{P}_\phi}$ and the circle of $\vec{V}_o$ rotation, as shown in figure 6. This is determined for each avoidance plane by solving the variables in equation (11) with $z_{vo} = 0$, where the $\{x_{vo}, y_{vo}\}$ is equal to the avoidance point $\{x_{avo}, y_{avo}\}$ that satisfies equation (16). There will a maximum of four solutions for the $\vec{V}_{avo}$ of the respected $\mathbf{VO}_{\mathbf{P}_\phi}$. No (zero) solution can be resulted in two conditions: if no part of the circle of $\vec{V}_o$ rotation is not included in $\mathbf{VO}_{\mathbf{P}_\phi}$, or if all part of the circle is included. The later condition happens when the ownship is too close to the obstacle, and should be prevented by conducting the avoidance maneuver well before the condition occurred.

$$x_{vo}^2 + y_{vo}^2 = V_o^2 \tag{16}$$

An additional precaution is added in the algorithm when handling multiple encounters, which is to only use $\vec{V}_{avo}$ points that are outside all other imminent $\mathbf{VO}_\phi$s. This is shown in Figure 6-b for a multiple-encounters situation, where only the two outermost points are valid $\vec{V}_{avo}$, from the total of six intersections of $\vec{V}_o$ with $\mathbf{VO}_\phi$.

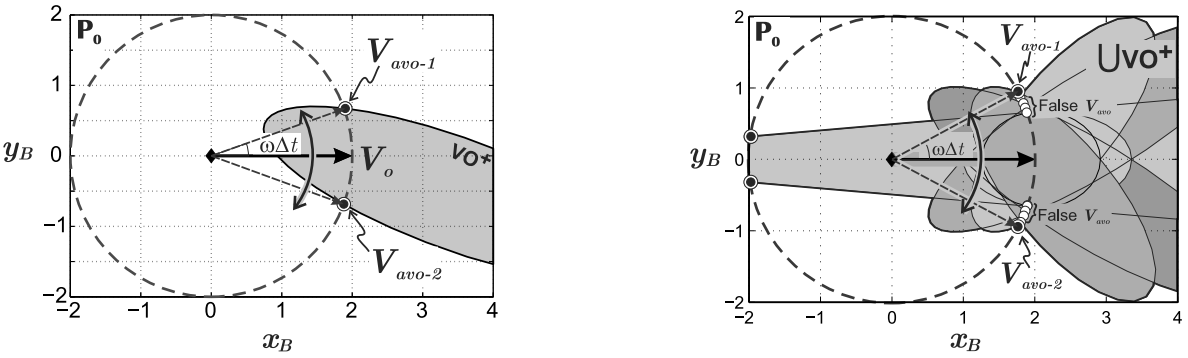

(a) (b)

Figure 6. The . (a).

B. Choosing an Avoidance Plane

To demonstrate the 3DVO method performance, this paper use an example of twleve Avoidance Plane, dicetized evenly around the ownship X-axis, from $-\pi/2$ to $\pi/2$. The ownship therefore can choose the best avoidance plane by comparing the angle of rotation from the current velocity vector $\vec{V}_o$ to the $\vec{V}_{avo}$ point on the respective $\mathbf{VO}_\phi$ section. The avoidance plane, however, can provide another information to refine this strategy, especially when taking into account the obstacle possible maneuver.

Besides the angle of rotations, the best Avoidance Plane can be chosen by considering the shape of the $\mathbf{VO}_\phi$ section. A degenerate triangular shape, for example, is generally more dangerous than an ellipse or a circle, since it indicates that the corresponding Avoidance Plane might be the same plane the obstacle are moving. Hence the avoidance maneuver can be nullified by an adverse movement of the obstacle. Hyperbolic $\mathbf{VO}_\phi$ sections also have the same dangerous tread, where it is possible that the obstacle is moving on the same plane, considering that the $\mathbf{VO}_\phi$ intersect the $\mathbf{VO}$ cone base as well.

For those reasons, the Avoidance Plane is chosen by weighing the danger of each plane base on the shape of the $\mathbf{VO}_\phi$ section. A Hyperbolic and triangular $\mathbf{VO}_\phi$ section are dropped, while ellipse sections are preferable, and therefore the avoidance is conducted in one of the $\mathbf{P}_\phi$ that have the particular shape. Afterwards the choice of $\mathbf{P}_\phi$ is based on which plane that can provide a $\vec{V}_{avo}$ with the smallest rotation angle. Note that eccentricity of the $\mathbf{VO}_\phi$ section is not used as a deciding factor (which would result a $\mathbf{P}_\phi$ that provide a section closest to of a circle), since it does not necessarily corresponds to the smallest rotation angle to a $\vec{V}_{avo}$.

In case of multiple encounters, the decision process is more tedious. The avoidance plane is chosen from those that can give a minimum level of dangerousness based on the inclusion of $\vec{V}_o$ and the shape of $\mathbf{VO}_\phi$, before deriving the one that have the smallest angle of rotation to a possible $\vec{V}_{avo}$. Note that even if a hyperbolic or triangular $\mathbf{VO}_\phi$ does not include the $\vec{V}_o$, the section is still considered more dangerous than an ellipse. However, the weight of a hyperbolic or triangular $\mathbf{VO}_\phi$ that includes the $\vec{V}_o$ is much larger, that should be outweighing every other section by a factor as large as the number of imminent obstacle.

C. Avoidance Turning Rate

Two parameters that needed to be defined to apply the algorithm for 3DVO are the avoidance distance d_{avo} and the avoidance turning rate ω_{avo}. The latter is required in an imminent encounter conflicts where the vehicle dynamics cannot be neglected.

Consider a between two vehicles, and ownship and an obstacle, initially positioned at $X_o(0)$ and $X_i(0)$, respectively, as shown in Figure 7. This type of conflict is considered as the worst scenario possible for an ownship, if it must conduct avoidance by turning to the opposite direction of the obstacle S_{pz}, or in this case, to the left. The turning radius required is the smallest compare to any other colliding scenario, and hence require the largest value of avoidance turning rate, ω_{avo}.

From the initial point at $T = 0$, the ownship follows a circular path with radius $r_{avo} = V_o/\omega_{avo}$, while the obstacle kept its straight trajectory. The vehicles meet at $T = t$, where the ownship grazes the obstacle protected zone, achieved by two conditions: the ownship position $X_o(t)$, is just at the edge of the S_{pz}, and its vector of velocity $V_o(t)$ exactly tangential to that circle. This meeting condition is achieved when the value of the ownship avoidance turning rate, $\omega_{a.cr}$ is critical: if it is bigger, the avoidance path will have some offset from the S_{pz} edge, and if it is smaller, the ownship will penetrate the protected zone. The critical value of ω_{avo} that is derived in the this worst case scenario should be able to ensure safety in the other scenario of conflict.

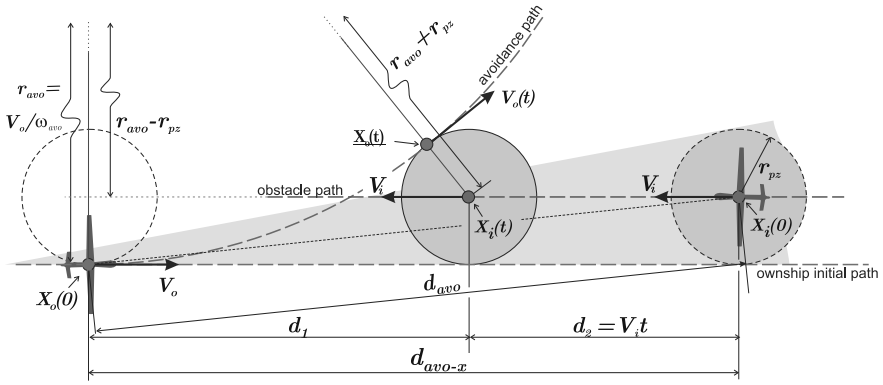

Figure 7. a

The relation between the critical value of the avoidance turning rate, $\omega_{a.cr}$, with the avoidance distance d_{avo}, can be derived by splitting it into two parts, the ownship part, d_o, and the obstacle part d_i. The former is derived using the critical conditions, which implies that the center of the circular avoidance path, the point of grazing, $X_o(t)$, and the center of the S_{pz} lies on one straight line. A right triangle, therefore, can be formed, with $r_{avo} + r_{pz}$ as the hypotenuse, and with $r_{avo} - r_{pz}$ and d_o as the legs. Hence the d_o can be expressed as a function of the conflict geometry, as presented in equation (18). The d_{avo} is then solved as the hypotenuse of the triangle with d_o and the S_pz radius as the legs, as presented in equation (17).

The obstacle part of the avoidance distance, d_i, is a straight line that can be derived by using the obstacle speed $|V_i|$ and the time, as expressed in (19). The time here, however, have to match the time the ownship require to reach point $X_o(t)$ from its initial position. To derive the required time, the ownship $V - o$ rotation can be used: from the initial heading, $\psi_o(0) = 0$, the ownship rotate using a constant turning rate ω_{avo} until $\psi_o(t) = \omega_{avo}t$, which corresponds directly to the opposite angle of d_o, in the right triangle before. Equation (20) expressed the time in terms of the turning rate and the encounter geometry.

$$d_{avo} = \sqrt{(d_o + d_i)^2 + r_{pz}^2} \tag{17}$$

$$d_o = \sqrt{(r_{avo} + r_{pz})^2 - (r_{avo} - r_{pz})^2} = 2\sqrt{\frac{V_o r_{pz}}{\omega_{avo}}} \tag{18}$$

$$d_i = V_i \Delta t \tag{19}$$

where,

$$\Delta t = \frac{1}{\omega_{avo}} \arctan\left(\frac{d_o}{r_{avo} - r_{pz}}\right) = \frac{1}{\omega_{avo}} \arctan\left(\frac{d_o}{V_o/\omega_{avo} + r_{pz}}\right) \tag{20}$$

Figure 8 shows the relation between the avoidance distance d_{avo} and the critical value of the avoidance turning rate $\omega_{a.cr}$, for worst case scenario explained before. The resulting curve is somewhat similar to the graph of the same parameter in Ref,[7] which is obtained using a different method. The Figure 8 is derived for a constant ownship speed of 5 m/s, facing obstacle with speed from 5 to 10 m/s. The radius of protected zone is of 1 meter. The required turning rate increase as the increment of the obstacle speed, which suggest that to provide an adequate turning rate, the ownship need to estimate first the speed of obstacle it might encounter during its operation. Furthermore, the $\omega_{a.cr}$ increases exponentially with the closer point of d_{avo} and practically set a minimum distance of avoidance for a range of obstacle's speed. If it is estimated that the obstacle would have speed up until 10 m/s, avoidance at 5 m from the obstacle, by a pure turning, would be impossible. These resulting $\omega_{a.cr}$ and the corresponding avoidance distances are used in the 3DVO implementation, presented in the next section.

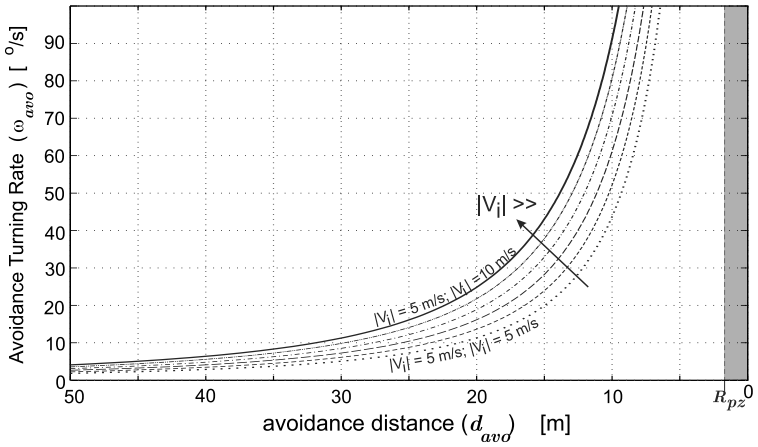

Figure 8. a

IV. Implementation

To evaluate its performance, the Three-dimensional Velocity Obstacle method is tested in three different simulated cases of three-dimensional encounters. The cases are designed to test the method on generating three-dimensional resolutions, on handling the maneuvering obstacles, and on handling multiple encounters. The simulations are presented using time-captures, where each vehicle protected zone, S_{pz} is represented by a sphere, and each vehicle velocity vector is visualized with a small cone.

A. Two Vehicles Converging

Figure 9 shows the simulation of the case that has been used to explain the 3DVO concept in previous sections, shown in Figure 2 to 3. This case serves as a proof of concept and the strategy of the 3D resolution generation using the avoidance planes. Two conflicting vehicles are involved in the case, where the ownship is using the 3DVO method and conduct avoidance at d_{avo} of 10 meters, while the obstacle, stays on its initial flight path. Both vehicle move at 5 meters/second in a straight line, heading to a goal point far away from the initial position.

From the twelve avoidance plane provided by the 3DVO strategy, four avoidance-planes, i.e., $\mathbf{P_{-90}}$, $\mathbf{P_{-45}}$, $\mathbf{P_0}$, and $\mathbf{P_{45}}$, are demonstrated. For each plane, both right and left turning are tested, making a total of eight resolution path for the encounter case, as shown in a composite time-lapse frame in Figure 9. Every resolution successfully avoid the obstacle, as shown by the distance between the two vehicle in Figure 10-a. An offset from the obstacle r_{pz} is resulted from the use of the buffer velocity set.

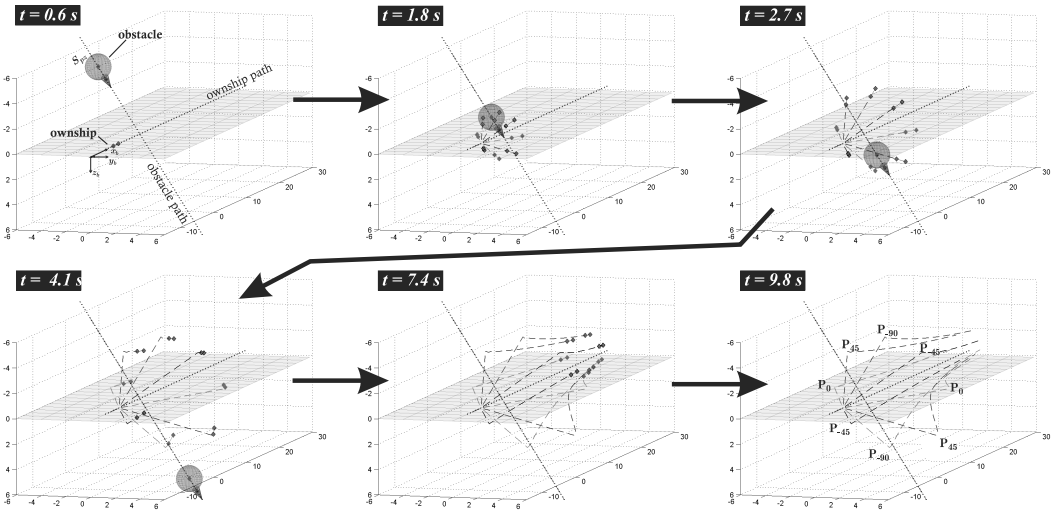

Figure 9. Simulation-1: The case shown in Figure. Several choices of avoidance plane are given, $\mathbf{P_{-90}}$, $\mathbf{P_{-45}}$, $\mathbf{P_0}$, and $\mathbf{P_{45}}$

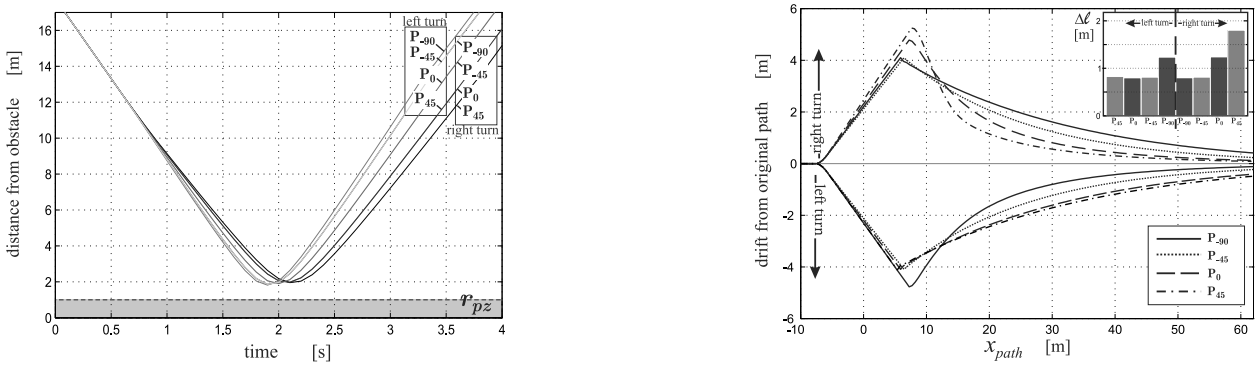

(a) (b)

Figure 10. Simulation-1: (a) Distance between vehicles and (b) Ownship drifting from original path for avoidance.

Figure 10-b shows the ownship drifting distance over time on each plane and each direction of avoidance. The figure shows almost the same maneuvering slope for every generated resolution. The vehicle drift from its initial path can be evaluated by calculating the total path length of the drifting profile, Δl, as shown in the inset of the figure 10-b. The value can be use to determine the efficiency of the avoidance maneuver. By comparison, turning to the right on $\mathbf{P_{45}}$ is the least efficient way to avoid for the encounter case. The more efficient way of avoidance is resulted by turning to the left on $\mathbf{P_{45}}$, $\mathbf{P_0}$ and $\mathbf{P_{-45}}$, or by turning to the right on $\mathbf{P_{-90}}$ and $\mathbf{P_{-45}}$, each differentiate by just a small margin. These results correspond to the $\mathbf{VO}_\phi$ section of each avoidance plane, shown in Figure 4-b, where the least efficient avoidance happen on the plane that have a triangular $\mathbf{VO}_\phi$ section, $\mathbf{P_{45}}$.

B. Multiple Heterogeneous Conflicts

This simulation is to test the overall capability of the 3DVO: generating resolution in a multiple and dynamic encounter situation. Here, eight vehicles are tested in a cube-like setup, as shown in Figure 11. Each sphere

in the figure represent half the radius of the protected zone to conserve the visualization of the collision, such that vehicle collisions are shown by two touching spheres, instead of two coincident spheres. This setup is a three-dimensional extension of the eight vehicle 'super-conflict' case used in previous studies[?,1] to test the two dimensional collision avoidance method.

The vehicles in this simulation are heterogeneous, meaning that each of them has different speeds, V and preference of where to start the avoidance, d_{avo}. The speed of each of the vehicles is given randomly within a range of 5 - 10 meters/second. While the d_{avo} is also given randomly within 10 - 15 meters, corresponding to the result of the critical turning rate in Figure 8. The initial positions in the cube are selected along the respecting space diagonals, to make all vehicles reach the center of the cube at the same time. The 3DVO method and strategy is used in each vehicle, which enables it to avoid others by choosing the avoidance plane with the smallest turning angle. With all obstacle avoiding in a random uncoordinated manner, the situation become dynamics: each vehicle are facing obstacle that can change direction at an arbitrary time. Figure 11 shows one example of the result for the scenario.

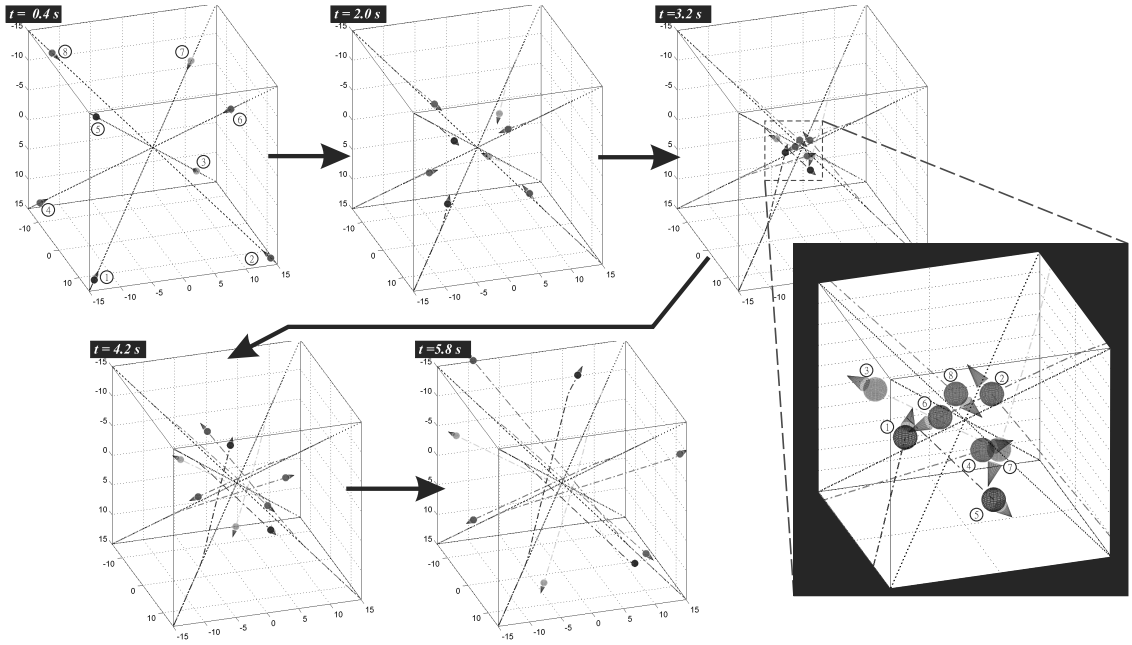

Figure 11. Simulation-4: Multiple 3-dimensional conflicts, in heterogeneous setup.

The simulation shows that the heterogeneous setup produces a variation of resolution maneuvers, which ultimately resolve the conflict independently for every vehicle. The work of the 3DVO can be represented by the change of the flight path and the heading angle, as shown in Figure 12. Here, each vehicle have different preference of avoidance, with vehicle-3 and -5 having the biggest change of attitude. The dynamic situations are shown by the modes of the vehicles, where the avoidance mode occurred more than one time for some of the vehicles. The change of attitude between the avoidance modes also demonstrate the variation of the avoidance-plane chosen during the maneuver, exploiting the three-dimensional space.

C. 3DVO Validation

This third implementation used to validate the performance of the 3DVO in generating three-dimensional resolution of various three-dimensional conflicts, using a series of Monte Carlo simulations. The eight vehicles super-conflict scenario in the previous subsection is used again with additional random factor for the vehicle position. As shown in Figure 13, besides the vehicles speeds and the avoidance distance, the global x, y and z position is also randomized, while keeping one representative vehicle in each octant of the euclidean space. The positions are then adjusted to force all vehicle to reach the origin at the same time. The speed and avoidance distance range is set within a range of 5 - 10 meters/second within 10 - 15 meters respectively. This scenario is generally more stressful than of the previous subsection, since the distances and spaces for avoidance decreases more rapidly.

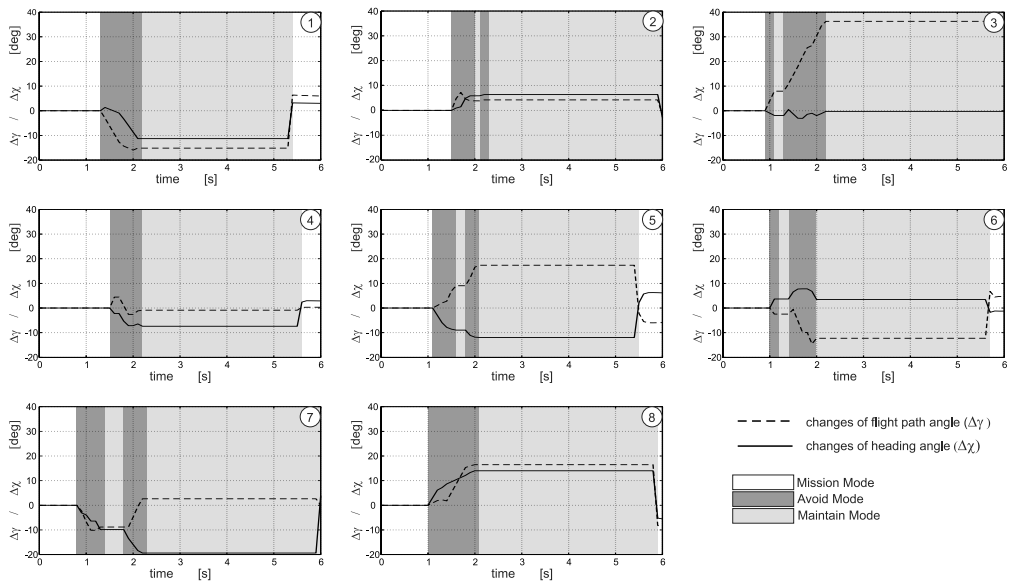

Figure 12. Cube-8 selecting Avo

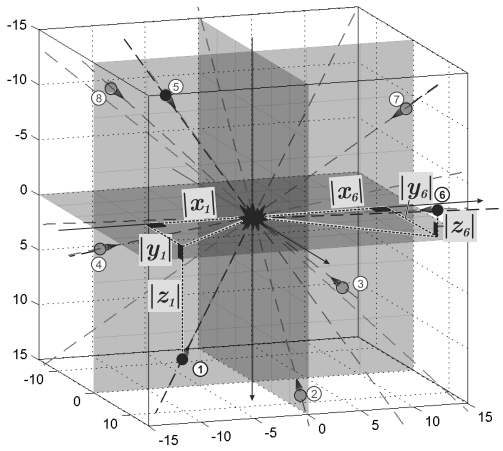

Figure 13. Cube-8 selecting Avo

The collision probability inside the space for a limited time frame is then calculated using the following equation (21). Along with the complete 3DVO method simulation, three other method of avoidance is also tested for comparison: (1) the two dimensional VO-method, where avoidance only happen on each vehicle XY-plane, (2) the same two dimensional VO-method but with the additional Buffer Velocity set to take account obstacle maneuvers, and (3) the three-dimensional VO-method but without the use of the Buffer Velocity set. A total of 25000 different initial condition samples, N_{MC}, are considered. The number is selected by observing the convergence of the P_{col} results for each series of simulation. Collision is marked when at least two vehicles distance is less then the designated radius $r_{pz} = 1$ meter, where the simulation is stopped and marked as a colliding sample, N_{col}. Any possible collision afterward is neglected. Note that the result does not follows one vehicle in particular, but rather the general probability in the setup 'super-conflict' scenario.

$$P_{col} = \frac{N_{col}}{N_{MC}} \tag{21}$$

The result of the Collision Probability is presented in the following table 1. It is shown that ttwo dimensional avoidance is not enough to solve a three-dimensional uncoordinated conflict. The use of more avoidance

plane, which exploit more the three-dimensional space gives lower collision probability, even without considering the obstacle maneuver. however, in the uncoordinated situation, the use of the Buffer Velocity set is proven to be necessary. Ultimately, in the 25000 samples tested, the 3DVO method and the proposed strategy are able to resolve all of the random three-dimensional, uncoordinated, dynamic multiple conflicts.

Table 1. Collision probability result comparison

	Number of Avoidance Plane	Use **BV**	Collision Probability
Method 1 (VO-method)	1	NO	5.75 %
Method 2	1	YES	1.02 %
Method 3	12	NO	1.04 %
Method 4 (3DVO)	12	YES	0 %

V. Conclusion

This paper has proposed a novel conflict resolution method called the Three Dimensional Velocity Obstacle Method (3DVO). The method is designed to generate a reactive three-dimensional avoidance maneuver for an Unmanned Aerial Vehicle (UAV) to avoid three-dimensional obstacles. The method takes into account the uncoordinated obstacles movement, as well as multiple obstacle encounters. The overall 3DVO method performance has been demonstrated using series of simulations, resulting zero collision in every designated conflict scenario.

A three-dimensional avoidance strategy has been presented, which has been developed based on the two key features of the 3DVO method: the addition of the Buffer Velocity zone, and the concept of the Avoidance Planes. The former ensure safety of the UAV in facing obstacle with adverse movement during the avoidance process, while the latter generates resolution by exploiting the available three dimensional space around the ownship, vastly reducing the possibility of collision. The calculation process involves an iteration for each avoidance plane, which can be limited to reduce the calculation time, based on the UAV capability.

While the 3DVO shows many promising results, there is still room for improvement. The method have yet to be tested in higher density of the 'super-conflict' cases. The uncertainties factor has yet to be considered, which is necessary for the designated conflict scenario that implies the use of on-board sensors. Real life flight testing are also mandatory before the 3DVO can be considered ready to be implemented in a UAV. Nevertheless, the 3DVO has been demonstrated and performed as intended for the designated scenario, which is one of the concerning factors toward UAVs integration into the airspace system.

References

[1]Hoekstra, J., van Gent, R., and Ruigrok, R., "Designing for Safety: the Free Flight Air Traffic Management Concept," *Reliability Engineering & System Safety*, Vol. 75, No. 2, 2002, pp. 215 – 232, doi: 10.1016/S0951-8320(01)00096-5.

[2]Fiorini, P. and Shiller, Z., "Motion Planning in Dynamic Environments Using Velocity Obstacles," *The International Journal of Robotics Research*, Vol. 17, No. 7, 1998, pp. 760–772, doi: 10.1177/027836499801700706.

[3]Kluge, B. and Prassler, E., "Recursive Probabilistic Velocity Obstacles for Reflective Navigation," *Field and Service Robotics*, edited by S. Yuta, H. Asama, E. Prassler, T. Tsubouchi, and S. Thrun, Vol. 24 of *Springer Tracts in Advanced Robotics*, Springer Berlin Heidelberg, 2006, pp. 71–79, doi: 10.1007/10991459_8.

[4]van der Berg, J., Lin, M., and Manocha, D., "Reciprocal Velocity Obstacles for Real-Time Multi-Agent Navigation," *International Conference on Robotics and Automation*, IEEE, Pasadena, CA, USA, 2008, doi:10.1109/ROBOT.2008.4543489.

[5]van Dam, S. B. J., Mulder, M., and Van Paassen, M., "Ecological Interface Design of a Tactical Airborne Separation Assistance Tool," *Systems, Man and Cybernetics, Part A: Systems and Humans, IEEE Transactions on*, Vol. 38, No. 6, Nov 2008, pp. 1221–1233, doi: 10.1109/TSMCA.2008.2001069.

[6]Heylen, F. M., van, S. B. J., Mulder, M., and van Paassen, M. M., "Design and Evaluation of a Vertical Separation Assistance Display," *AIAA Guidance, Navigation, and Control Conference and Exhibit*, Honolulu (HI), 2008, AIAA 2008-6969, doi:10.2514/6.2008-6969.

[7]Snape, J., van den Berg, J., Guy, S., and Manocha, D., "The Hybrid Reciprocal Velocity Obstacle," *Robotics, IEEE Transactions on*, Vol. 27, No. 4, Aug 2011, pp. 696–706, doi: 10.1109/TRO.2011.2120810.

[8]Kluge, B., "Recursive Probabilistic Velocity Obstacles for Reflective Navigation," *Proc. of 1st Int. Workshop on Advances in Service Robots.*, 2003.

[9]Mao, Z.-H., Feron, E., and Bilimoria, K., "Stability and performance of intersecting aircraft flows under decentralized conflict avoidance rules," *Intelligent Transportation Systems, IEEE Transactions on*, Vol. 2, No. 2, Jun 2001, pp. 101–109, doi:10.1109/6979.928721.

[10]Hurley, R. D., Lind, R., and Kehoe, J. J., "A Torus Based Three Dimensional Motion Planning Model for Very Maneuverable Micro Air Vehicles," *AIAA Guidance, Navigation, and Control Conference 2013*, AIAA, Boston, MA, 2013, AIAA 2013-4938, doi:10.2514/6.2013-4938.

This is a self-archived version. Please find the completed version of this paper at http://arc.aiaa.org/doi/abs/10.2514/6.2016-1629 (doi:10.2514/6.2016-1629) - note: the JGDC journal version already published! (doi:10.2514/1.G001715)